Purdue University

Purdue e-Pubs

International Compressor Engineering
Conference

School of Mechanical Engineering

2024

Geometric and Numerical Investigation of Twin-Screw Vacuum Pumps

Yang Lu
yang.lu.8@city.ac.uk

Sham Rane
sham.rane@city.ac.uk

Ahmed Kovacevic
a.kovacevic@city.ac.uk

Follow this and additional works at: https://docs.lib.purdue.edu/icec

Geometric and Numerical Investigation of Twin-Screw Vacuum Pumps

Yang LU[1]*, Sham Rane[1], Ahmed Kovacevic[1]

[1] City, University of London, School of Science and Technology,
London, United Kindoom
Contact Information (yang.lu.8@city.ac.uk)

* Corresponding Author

ABSTRACT

This paper presents analysis of twin-screw vacuum pumps, encompassing both geometrical calculations and numerical simulations. The geometrical calculations include key parameters such as chamber volume, leakage area, suction port area, and discharge port area. These parameters are studied across rotational angles for constant pitch, and stepped pitch configurations. The leakage areas include radial, axial, and interlobe leakage paths. Computational Fluid Dynamics (CFD) is employed to investigate the axial leakage paths. Additionally, the study utilizes the SCORG software package, an inhouse simulation tool to calculate thermodynamic processes and integral parameters. By integrating the geometric calculations into SCORG, this approach enables extensive calculation and design optimization of twin-screw vacuum pumps. Five different combinations of pitch were analyzed to assess their impact on both volume flow rate and efficiency. The analysis revealed that reducing the pitch of the second stage resulted in a decrease of approximately 2% in volumetric efficiency, while adiabatic efficiency increased by around 4%. The findings contribute to a more comprehensive understanding of the performance characteristics and design considerations for twin screw vacuum pumps.

1. INTRODUCTION

Vacuum technology plays a pivotal role in a myriad of industrial applications, spanning from semiconductor technology to food packaging and freeze drying (Jousten, 2016). Vacuum pumps for these applications operate at a broad pressure range, from 10^{-10} Pa for extreme vacuum conditions to 10^5 Pa at atmospheric pressure. Positive displacement machines, such as roots vacuum pumps, scroll vacuum pumps, and twin screw vacuum pumps could be used to operate in both rough and fine vacuum regimes ($10^2\ to\ 10^{-1}\ Pa$). Oil-free twin screw vacuum pumps have emerged as a popular choice, characterized by features such as variable pitch, large wrap angle, and a discharge port plate, enabling operation at lower suction pressures. While previous studies on twin screw vacuum pumps have primarily focused on rotor profile design (Li, He, Wu, et al., 2022; Lu et al., 2015; Stosic et al., 2016) and performance modelling (Li, He, Sun, et al., 2022; Li et al., 2021; Li, He, Wang, et al., 2022; Li, He, Wu, et al., 2022; Pfaller et al., 2011; Pleskun et al., 2021), it's crucial to note that simulations have typically overlooked axial leakage and discharge port considerations. Consequently, the accuracy of simulation results may be compromised, as axial leakage losses and discharge losses significantly impact power consumption and volume flow rate. In this paper, all leakage paths, including radial, axial, and interlobe leakage flows were addressed. Furthermore, variations in discharge port area with rotational angle were calculated. Leveraging the chamber model utilized for twin screw compressors, thermodynamic calculations are tailored for twin screw vacuum pumps. Finally, different pitch combinations were compared to assess their impact on the volume flow rate and indicated power, offering insights into optimizing twin screw vacuum pump performance.

2. GEOMETRY CALCULATION

The geometric characteristics of twin-screw vacuum pumps include chamber volume, leakage area and port area. In order to construct an accurate performance chamber model, it is imperative to calculate geometric characteristics in advance. In this section, it begins by introducing the design parameters of rotor geometry. Subsequently, the calculation of chamber volume for both constant pitch and variable pitch configurations is presented. Leakage areas

are computed, with particular emphasis placed on analyzing the axial leakage path using Computational Fluid Dynamics (CFD) methodology. Additionally, the variation in suction port area and discharge port area with rotational angle is determined.

In this section, the introduction of geometrical parameters essential for thermodynamic calculations is detailed. These parameters encompass chamber volume, leakage area, and port area. Chamber volume calculations are applicable across various pitch configurations, including constant pitch, stepped pitch, and linear pitch. Additionally, the intricate calculations involved in determining leakage areas, which comprise radial leakage, axial leakage, and interlobe leakage, are explored. Moreover, the variations in suction port area and discharge port area are considered.

2.2 Chamber volume
First of all, the cross-section area between rotor and casing is calculated. Then chamber volume is integrated by times the area of cross section and $Z_i - Z_{i-1}$ as shown in the following equation.

$$Chamber\ Volume = \sum A_i(Z_i - Z_{i-1}) \tag{1}$$

In a twin-screw machine, the pitch refers to the distance between corresponding points on adjacent lobes of the rotor. It is commonly defined as the axial distance traveled by the rotor for one complete revolution. The pitch can either remain constant, meaning it stays the same along the length of the rotors, or it can vary depending on the design of the vacuum pumps. In certain instances, the pitch may change gradually or stepwise along the length of the rotors to optimize performance for specific operating conditions. The options for rotor pitch type typically include uniform, variable, and stepped. While a uniform pitch is easier to manufacture, both variable pitch and stepped pitch designs offer gradual compression. Stepped pitch can be optimized for different stages of the working process, providing a cost-effective solution. In contrast, variable pitch is ideal for applications that require high efficiency and smooth operation. Figure 1 illustrates these three types of pitch. For the purposes of this research, we will focus on studying the stepped pitch configuration.
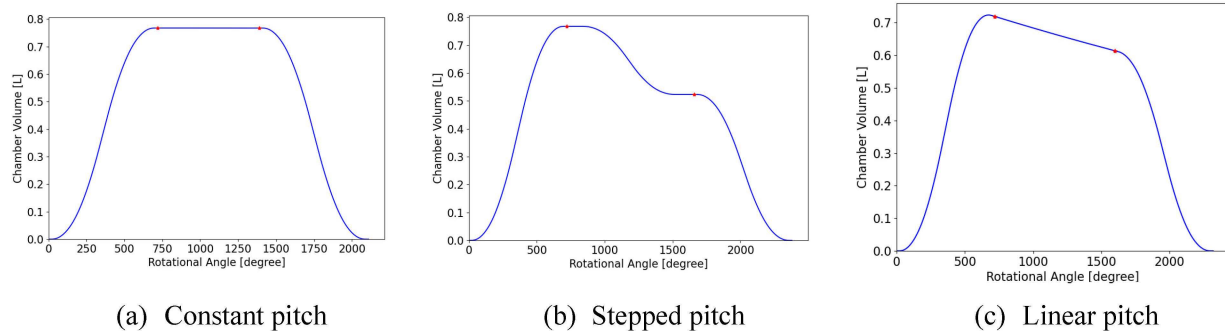

| (a) Constant pitch | (b) Stepped pitch | (c) Linear pitch |

Figure 1: Chamber volume of different pitch type

2.3 Leakage area
Leakage paths encompass radial, axial, and interlobe leakage. Their respective areas can be computed by multiplying the length of the leakage path by the gap size as shown in equation (2). Radial leakage area is determined by rotor tip length, while interlobe leakage area is calculated based on the sealing line length. In this study, axial leakage is investigated using Computational Fluid Dynamics (CFD) methodology.

$$Leakage\ area = \sum gap(Z_i - Z_{i-1}) \tag{2}$$

For the CFD simulation, the fluid domain of constant pitch main and gate rotors with a wrap angle of 720 degrees have been generated as shown in Figure 2. The rotor length is set at 144 mm, while the axial gap size measures 100 μm with no radial gap present. A mesh comprising five layers is generated at the axial gap. The simulation is transient, with 500 timesteps and a timestep size of 1E-05 s. Inlet pressure is specified as 1 bar, while the discharge pressure is set at 3 bar.
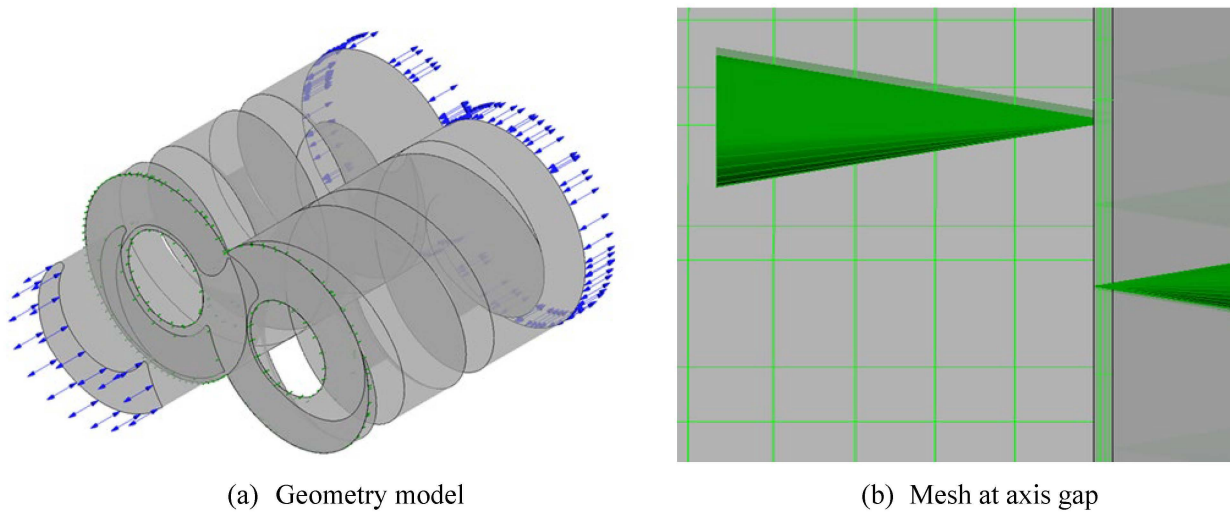
(a) Geometry model   (b) Mesh at axis gap

Figure 2: CFD model for axial leakage analysis

In the configuration of 36 cases with different rotor rotational positions, six featured rotational positions have been selected to demonstrate the axial leakage paths. These phases are distinguished based on the contact line: Two range of pressure contour are selected to show the pressure difference. Phase 1, where the contact line is at the main rotor's outer circle, exhibits two leakage paths spanning the length of the addendum plus dedendum. Phase 2, occurring between the two rotors, presents three leakage paths, each with the same length as in Phase 1. Finally, Phase 3, with the contact line at the gate rotor's outer circle, showcases two leakage paths of similar length to those in Phase 1.
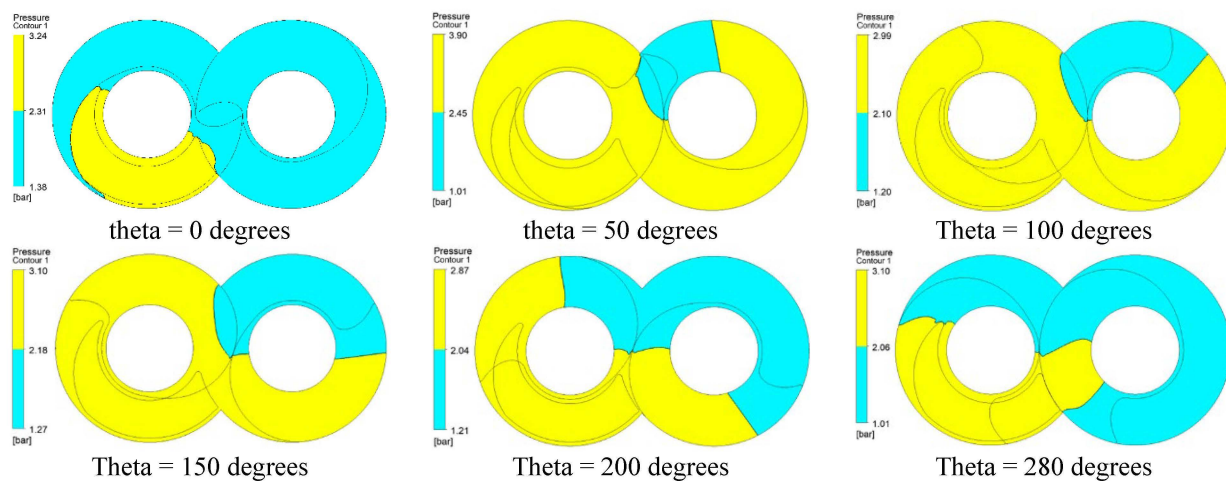

Figure 3: CFD results to show axial leakage path

Interlobe leakage area is determined by analyzing the contact line. Three distinct leakage areas are computed and compared in Figure 4. All three leakage paths are configured with identical gap sizes for stepped pitch case. Notably, the radial leakage area surpasses the interlobe leakage area, while the axial leakage area registers as the smallest among the three.
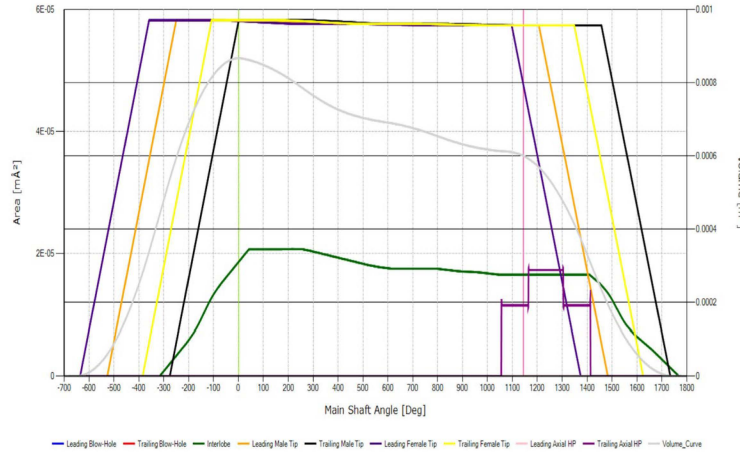
Figure 4: Leakage area

2.4 Discharge port area

Discharge port area can be calculated based on the design of the built-in Volume index (Vi). Different port geometry can be automatically calculated based on the Vi and given rotor profile as shown in Figure 5. Three distinct discharge ports are created based on the provided Vi. As Vi increased, the size of discharge port was reduced.
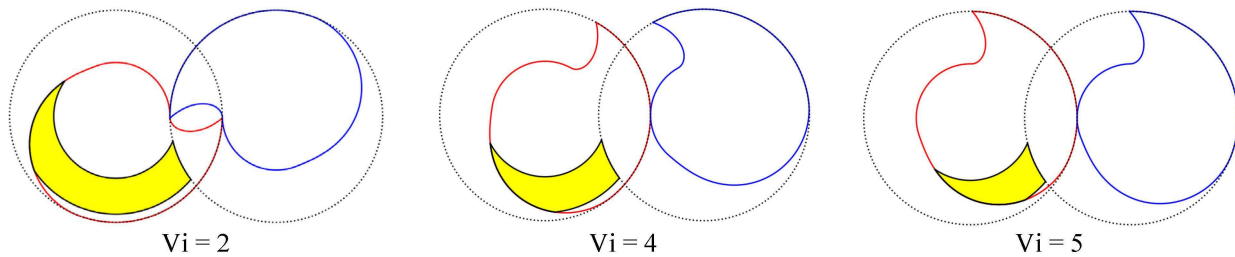

| Vi = 2 | Vi = 4 | Vi = 5 |

Figure 5: Discharge port area

A numerical procedure was employed to compute the time-varying flow area of the discharge port. The flow path between the working and discharge chambers initiates when the edge C3 of the rotor lobe intersects the opening curves of the discharge port. Initially, the flow area starts at zero and progressively increases to its maximum extent. Subsequently, it diminishes until the rotor lobe completely seals off the connection between the working chamber and the discharge port. This process is analyzed by defining numerous small elemental areas positioned between adjacent radii and the port boundaries, as depicted in Figure 6. The total flow area through the axial discharge port is determined by summing all these elemental areas.
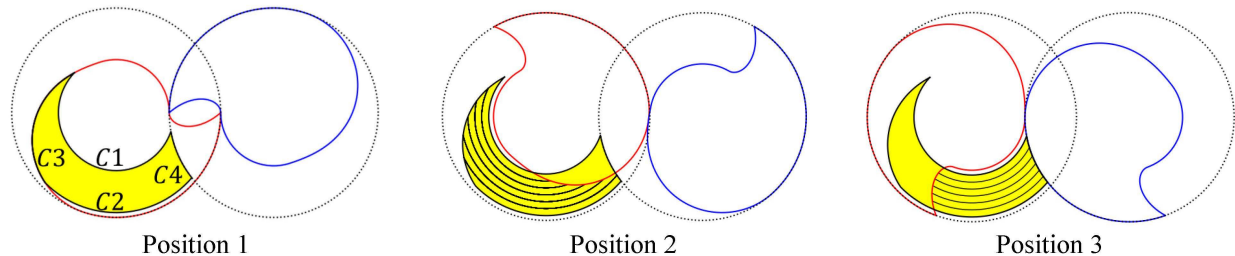

| Position 1 | Position 2 | Position 3 |

Figure 6: Discharge port area

Suction and discharge port area changing with rotational angle can be calculated as shown in Figure 7. The blue curve shows the suction port area changing with rotational angle while green curve shows discharge port area changing with rotational angle. Gray curve shows the chamber volume changing with rotational angle. Since the

suction port is fully opened for twin screw vacuum pump, the area changing of suction port is same as cross section area changing between two rotors and casing.
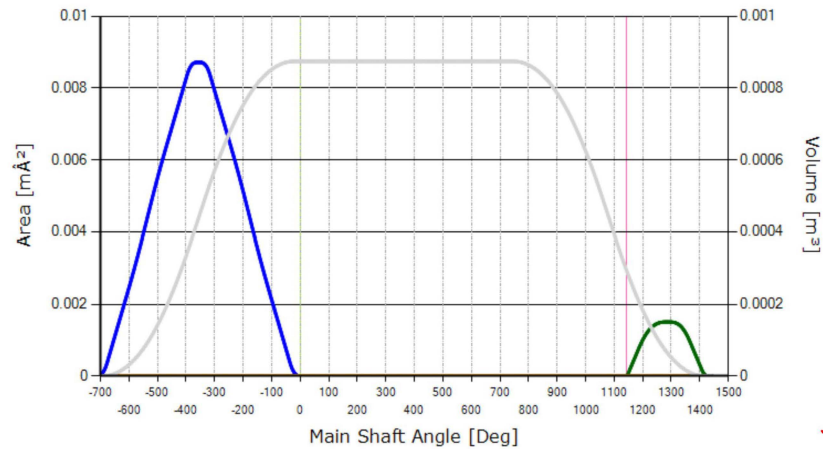

Figure 7: Suction and discharge port area

3. NUMERICAL SIMULATION

The geometry calculations have been incorporated into SCORG, which houses the thermodynamic model utilized for twin screw compressor calculations. This identical thermodynamic model is also applied for twin screw vacuum pump calculations (Stosic et al., 2005). Notably, the simulation does not account for bearing losses or sealing losses. The primary objective of this simulation is to explore the influence of pitch combinations on performance outcomes.

Five cases have been meticulously analyzed utilizing the refined geometry model. In each case, consistent parameters such as a wrap angle of 1440 degrees and a Vi (internal volume index) of 3 have been maintained. Moreover, to ensure uniform displacement within the vacuum pump, the pitch of the first proportion remains unchanged as 100 mm, while the second pitch is systematically reduced across all cases from 100 mm to 65 mm. The displacement of the studied twin screw vacuum pump is 0.875 L/rev. To maintain uniform wrap angles across the configurations, adjustment is complemented by a proportional reduction in rotor length as shown in Table 1.

Table 1: Rotor geometry

Parameters	Unit	Case1	Case2	Case3	Case4	Case5
Length	[mm]	400	360	350	340	330
Wrap angle	[degree]	1440	1440	1440	1440	1440
Pitch_1	[mm]	100	100	100	100	100
Pitch_2	[mm]	100	80	75	70	65
Proportion_1	[/]	0.5	0.56	0.57	0.588	0.606
Proportion_2	[/]	0.5	0.44	0.43	0.412	0.394

The operational parameters for thermodynamic calculations are outlined in Table 2. A rotational speed of 8000 rpm is maintained, with a suction pressure of 0.1 bar and a discharge pressure of 1 bar. Notably, the suction pressure is deliberately set below the fine vacuum pressure range, as the chamber model initially developed for twin screw compressors may lack precision under fine vacuum conditions. Additionally, it's worth noting that the gap size for all three leakage paths is uniformly set to 50 μm.

Table 2: Working condition

Parameters	Unit	Value
Speed	[rpm]	8000
P_suc	[bar]	0.1
P_dis	[bar]	1
T_suc	[K]	293
Vi	[/]	3

Figure 8 illustrates pressure curves of Case 2, providing the pressure changing of variable pitch case. Notably, the pressure within the control volume experiences a gradual increase, with small discharge pressure losses when the control volume connects with the discharge port. Examination of the pressure-volume curve reveals a distinct pressure jump during the compression process. This phenomenon can be attributed to the stepped pitch design, which induces variations in pressure levels within the system.
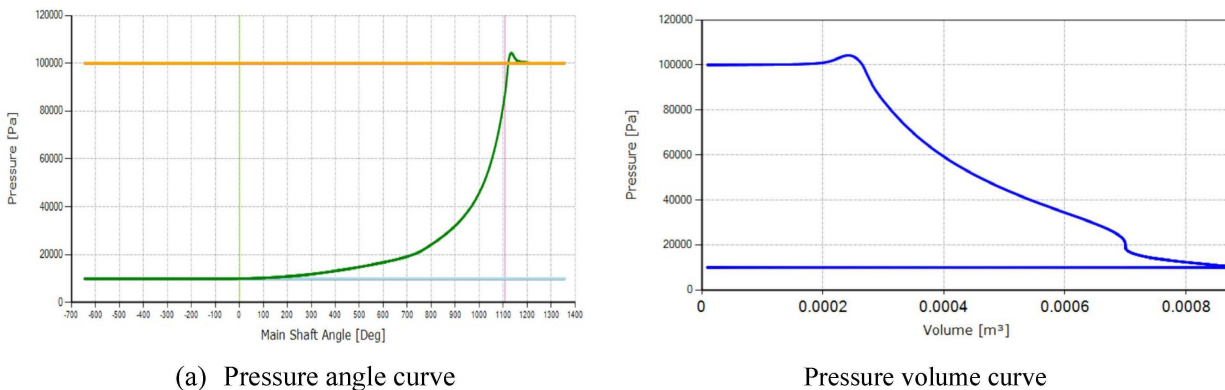

(a) Pressure angle curve   Pressure volume curve

Figure 8: Pressure curve

Table 3 presents a comparison of key performance metrics including volume flow rate, indicated power, volumetric efficiency, adiabatic efficiency, and specific power across Cases 1 to 5. It is observed that both volume flow rate and volumetric efficiency decrease from Case 1 to Case 5. This reduction can be attributed to the higher internal volume ratio resulting from the decreased second portion of the pitch. Higher internal volume ratios typically lead to increased leakage. However, adiabatic efficiency exhibits an opposite trend, showing an increase across the cases. This can be attributed to two primary factors. Firstly, the compression process tends to be more isothermal. The enclosed area of pressure volume curve is expected to reduce from Case1 to Case 5. Additionally, the lower discharge losses associated with larger discharge ports contribute to this observed increase. Notably, specific power demonstrates a decreasing trend from Case 1 to Case 5, indicating an improvement in efficiency across the configurations.

Table 3: Performance comparison

Parameters	Unit	Case1	Case2	Case3	Case4	Case5
Q	[m3/min]	6.79	6.66	6.65	6.65	6.65
P_ind	[kW]	5.93	5.67	5.60	5.55	5.48
ηv	[%]	97.05	95.19	95.01	94.98	94.99
ηad	[%]	62.13	63.82	64.62	65.05	65.82
Specific power	[kW/m3/min]	0.874	0.851	0.843	0.835	0.825

4. CONCLUSIONS

This paper undertakes calculations of key geometrical parameters, including chamber volume, leakage area, and discharge port area. Leveraging the chamber model employed for thermodynamic calculations in twin screw compressors, the application is extended to twin screw vacuum pumps. The study involves comparing five different pitch combinations in terms of volume flow rate, indicated power, volumetric efficiency, adiabatic efficiency, and specific efficiency. The simulation results demonstrate a noteworthy trend: by reducing the second proportion pitch,

volumetric efficiency is observed to decrease while adiabatic efficiency tends to increase. Specifically, volumetric efficiency experiences a reduction of approximately 2%, whereas adiabatic efficiency sees an increase of around 4%. These findings underscore the benefits associated with reducing the second proportion of pitch in twin screw vacuum pump configurations.

NOMENCLATURE

P_ind	indicated power	(kW)
Q	volume flow rate	(m3/min)
Vi	volume index	(/)
ηv	volumetric efficiency	(%)
ηad	adiabatic efficiency	(%)

REFERENCES

Jousten, K. (2016). *Handbook of Vacuum Technology*. Wiley-VCH.

Li, D., He, Z., Sun, S., & Xing, Z. (2022). Dynamic characteristics modelling and analysis for dry screw vacuum pumps. *Vacuum*, *198*. https://doi.org/10.1016/j.vacuum.2022.110868

Li, D., He, Z., Wang, C., Guo, Y., Wei, W., Lin, D., & Xing, Z. (2021). Design methodology and performance analysis of conical rotors for dry screw vacuum pumps. *Vacuum*, *185*. https://doi.org/10.1016/j.vacuum.2020.110025

Li, D., He, Z., Wang, C., Sun, S., Ma, K., & Xing, Z. (2022). Simulation of dry screw vacuum pumps based on chamber model and thermal resistance network. *Applied Thermal Engineering*, *211*. https://doi.org/10.1016/j.applthermaleng.2022.118460

Li, D., He, Z., Wu, W., & Xing, Z. (2022). Study on the Quimby-tooth rotor profile for dry screw vacuum pumps. *Proceedings of the Institution of Mechanical Engineers, Part E: Journal of Process Mechanical Engineering*, *236*(5), 1947-1957. https://doi.org/10.1177/09544089221081334

Lu, Y., Guo, B., & Geng, M. F. (2015). *Study on Design of Rotor Profile for the Twin Screw Vacuum Pump with Single Thread Tooth* IOP Conference Series: Materials Science and Engineering,

Pfaller, D., Brümmer, A., & Kauder, K. (2011). Optimized rotor pitch distributions for screw spindle vacuum pumps. *Vacuum*, *85*(12), 1152-1155. https://doi.org/10.1016/j.vacuum.2011.03.002

Pleskun, H., Jünemann, T., Bode, T., & Brümmer, A. (2021). Modelling of inhomogeneous chamber states in rotary positive displacement vacuum pumps. *IOP Conference Series: Materials Science and Engineering*, *1180*(1), 012009. https://doi.org/10.1088/1757-899X/1180/1/012009

Stosic, N., Rane, S., Kovacevic, A., & Smith, I. K. (2016). *Screw Rotor Profiles of Variable Lead Vacuum and Multiphase Machines and Their Calculation Models* Volume 6A: Energy,

Stosic, N., Smith, I. K., & Kovacevic, A. (2005). *Screw Compressor Geometry_Mathematical Modeling and Performance Calculation*. Springer

ACKNOWLEDGEMENT